



HAL
open science

Shunt loudspeaker using nonlinear energy sink

Diala Bitar, Emmanuel Gourdon, Claude-Henri Lamarque, Manuel Collet

► **To cite this version:**

Diala Bitar, Emmanuel Gourdon, Claude-Henri Lamarque, Manuel Collet. Shunt loudspeaker using nonlinear energy sink. *Journal of Sound and Vibration*, 2019, 456 (2), pp.254-271. 10.1016/j.jsv.2019.05.021 . hal-02380424

HAL Id: hal-02380424

<https://hal.science/hal-02380424>

Submitted on 25 Oct 2021

HAL is a multi-disciplinary open access archive for the deposit and dissemination of scientific research documents, whether they are published or not. The documents may come from teaching and research institutions in France or abroad, or from public or private research centers.

L'archive ouverte pluridisciplinaire **HAL**, est destinée au dépôt et à la diffusion de documents scientifiques de niveau recherche, publiés ou non, émanant des établissements d'enseignement et de recherche français ou étrangers, des laboratoires publics ou privés.



Distributed under a Creative Commons Attribution - NonCommercial 4.0 International License

Shunt loudspeaker using nonlinear energy sink

D. Bitar^{a,b}, E. Gourdon^a, C.-H. Lamarque^a, M. Collet^b

^a*LTDS-UMR CNRS 5513, Ecole Nationale des Travaux Publics de l'Etat (ENTPE),
Univ. Lyon, 3 rue Maurice Audin, 69120 Vaulx-en-Velin cedex, France.*

^b*LTDS-UMR CNRS 5513, Ecole Centrale de Lyon (ECL), 36 avenue Guy de Collongue,
69134 Ecully Cedex, France.*

Abstract

The present paper aims to apply the concept of energy pumping for noise reduction at propagation and reception paths. This phenomenon consists in irreversible energy transfer from a linear primary system to a nonlinear energy sink, where the energy is finally dissipated. In this study, we turn a loudspeaker to an electroacoustic absorber by connecting at its transducers terminals a passive nonlinear shunt circuit playing the role of an absorber. The equivalent model consists of a linear structure describing the displacement of the loudspeaker, linearly coupled to a cubic nonlinear energy sink. For the case of 1:1 resonance, the Invariant manifold approach is applied for different time scales. It enables the detection of the slow invariant manifold and equilibrium and fold singularities at the fast and slow time scales respectively. This methodology provides a predictive tool allowing the design of the nonlinear energy sink for better control of the main system. The analytical and numerical results show that the nonlinear shunt circuit managed to expand the frequency band of the controlled system.

Keywords: Electroacoustic absorber, multiple time scales, nonlinear energy sink, nonlinear passive shunt.

Email addresses: diala.bitar@entpe.fr (D. Bitar), emmanuel.gourdon@entpe.fr (E. Gourdon), claudel.lamarque@entpe.fr (C.-H. Lamarque), manuel.collet@ec-lyon.fr (M. Collet)

1. Introduction

Excessive use of transportation, machinery, sound systems and so on, in parallel with the high demands of sound comfort and health care, encouraged researchers to achieve the noise reduction challenge. Several procedures are used in order to reduce noise at the propagation and reception paths. For instance, classical passive systems as sound absorbing materials such as porous and adaptive liners have been found to be very efficient at high frequencies in controlling room noise in building technologies [1]. However, these solutions are less efficient at mid and low frequencies in addition to their size. One of the best solutions that can be employed for these frequencies is to couple the treated system with linear resonating one, playing the role of an absorber. As an example, we can mention the Dynamic Vibration Absorbers (DVA) such as Helmholtz resonators [2] and Frahm dampers [3] which consist of a tuned spring-mass systems. Although these techniques can give perfect absorption, they can only treat very narrow frequency band [4]. Later on, the concept of active noise absorption has been introduced based on controlling a secondary source in order to cancel the primary sound wave. This concept opened the way to a large variety of active sound absorption techniques. We can mention feedback control based on sound pressure control of a loudspeaker [5, 6], the direct impedance control combining both sound pressure and diaphragm velocity sensing [7] allowing a broad frequency control. In addition, it has been proposed to employ a pure electrical network as a second source to maximize the absorption efficiency under the concept of shunt loudspeaker [8]. For low-frequency noise absorption, a passive shunt electric circuit connected to the coil and powered by a DC source was employed by Zhang et al. [9] allowing to modify the mechanical impedance of the coil, where Tao et al. [10] implemented a Micro-perforated panel backed by a shunted loudspeaker. Moreover, in a Rijke-tube an electroacoustic control device was experimentally and numerically tested as an alternative damping approach for suppressing the thermoacoustic instability [11].

Recent studies have shown that the performances of DVAs can be improved by employing nonlinear strategies. In fact, it has been shown in [12, 13, 14, 15] that employing nonlinear absorbers enables to absorb more efficiently the sound or vibrations at higher frequency band. This conceptual approach is based on irreversible energy transfer from a primary linear structure and nonlinear oscillator with small mass. This phenomenon is called targeted energy transfer or energy pumping, where the Nonlinear Energy

38 Sink (NES) may serve as a nonlinear absorber [16, 17]. This procedure has
39 achieved success in the mechanical field, where nonlinear phenomena were
40 exploited to reduce vibrations [18]. This concept was applied in the field of
41 acoustics, providing a new technique of passive absorption for low frequencies
42 [19].

43 However, this previous work [19] deals with very low frequencies with an
44 absorber that is not essentially nonlinear. For this purpose, we suggest to
45 switch a loudspeaker from its primary quality of diffusing sound and con-
46 vert it into an electroacoustic absorber as a technical solution to achieve
47 the desired nonlinear acoustical behavior. The general concept is to control
48 the acoustical impedance a membrane, which can be achieved by tuning the
49 dynamic of the loudspeaker membrane by connecting an appropriate elec-
50 trical load. This approach allows reaching almost perfect absorption within
51 a narrow frequency bandwidth around the resonance by employing a simple
52 optimal passive electric resistance [8]. In addition, it has been shown that
53 the bandwidth of control can be increased by choosing appropriate feedback
54 gains in a combined pressure-velocity-feedback or by coupling the primary
55 loudspeaker to a combination of several resonators [20]. Hence, the goal of
56 the present work consists in performing a purely acoustic nonlinear absorber
57 acting on low frequency domain, by connecting to the loudspeaker terminals
58 an electric nonlinear circuit that can be controlled. To our knowledge, it is
59 the first attempt to apply the concept of targeted energy transfer to an elec-
60 troacoustic absorber. Hence, this study aims at first to test the feasibility of
61 the concept, where the non-optimal nonlinear results were compared to the
62 ones obtained via an optimal linear resistor.

63 The present work is organized as follows: In section 2, we describe the
64 electroacoustic absorber consisting of loudspeaker shunted with an electrical
65 circuit. In section 3, an electroacoustic absorber consisting of a loudspeaker
66 coupled with a nonlinear electrical shunt circuit at its terminals has been
67 considered. The equivalent model is described by a 2 dofs system, includ-
68 ing the main linear oscillator characterizing the dynamics of the loudspeaker
69 membrane, which is linearly coupled to a cubic NES. In section 4, the Slow
70 Invariant Manifold (SIM) approach has been employed. The differential sys-
71 tem has been treated analytically for the case of 1:1 resonance at various
72 time scales [21]. The present methodology allows to identify the equilib-
73 rium points and fold singularities at the first slow time scale. In addition,
74 it provides a predictive tool to design an optimize nonlinear electric circuit
75 according to the energy exchange process between both systems. Section 5

76 provides an analytical expression allowing the identification of the different
 77 mechanisms of energy exchange in the case of free oscillations. In section 6,
 78 a physical application is considered presenting the advantage of combining a
 79 nonlinear electric shunt circuit to the loudspeaker terminals. Several analyt-
 80 ical and numerical results are given in the case of free and forced vibrations,
 81 allowing a global understanding of the presented approach and the possible
 82 behaviors that can be obtained. Finally, conclusions and perspectives are
 83 given in section 7.

84 2. Electroacoustic absorber description

85 At the beginning, we consider an electroacoustic absorber (see Figure 1)
 86 following the same concept of Lissek et al. in [8, 22]. The physical model
 87 provides insight into the loudspeaker parameters that can be affected by
 88 electrical means.

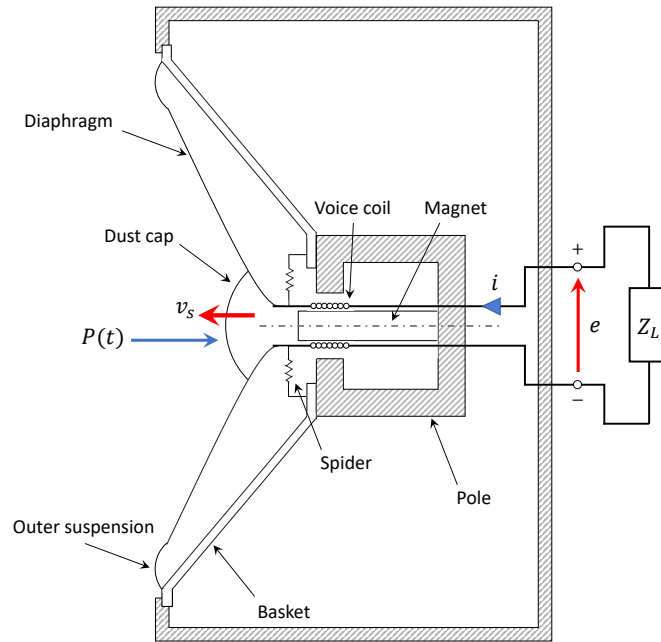


Figure 1: Shunt loudspeaker [22]

89 The mechanical dynamics of a loudspeaker diaphragm for small ampli-
 90 tudes and below the first modal frequency can be modeled by the following
 91 differential equation [derived from Newton's second law](#)

$$SP(t) = M_{ms}\dot{v}_s(t) + R_{ms}v_s(t) + \frac{1}{C_{ms}} \left(\frac{1}{C_{ms}} + \frac{\rho c^2 S^2}{V_b} \right) \int v_s(t) dt - Bl i(t). \quad (1)$$

~~92 M_{ms} , R_{ms} and C_{ms} are respectively the mass, the mechanical resistance~~
~~93 and the compliance of the moving bodies of the loudspeaker. C_{ms} is dened~~
~~94 so that $1/C_{mc} = 1/C_{ms} + \rho c^2 S^2/V_b$ is the equivalent compliance of the en-~~
~~95 closed loudspeaker (due to the closed box at the rear side of the loudspeaker).~~
~~96 V_b represents the enclosure volume, S the diaphragm area, ρ the density of~~
~~97 the medium and c the celerity of sound in the medium. The mechanical~~
~~98 moving part of the loudspeaker made of the suspended diaphragm and coil~~
~~99 is assimilated to a simple mass-spring-damper system with M_{ms} describing~~
~~100 the mass, C_{ms} accounting for the surround suspension and the spider and~~
~~101 R_{ms} the mechanical resistance. Equation (1) describes the motion of the~~
~~102 closed-box loudspeaker with S denoting the effective piston area and V_b the~~
~~103 volume of the cabinet. Then, the reaction of the fluid acting on the rear face~~
~~104 is modelled by $\rho c^2 S^2/V_b$ as a mechanical compliance of the cabinet, where~~
~~105 ρ representing the density and c the celerity of sound in the medium. $v_s(t)$~~
~~106 is the outgoing diaphragm velocity, Bl is the force factor of the moving-coil~~
~~107 transducer with B representing the magnetic field magnitude and l the length~~
~~108 of the wire in the voice coil. $i(t)$ is the driving current, $Bl i(t)$ the Laplace~~
~~109 force induced by the current circulating through the coil. $P(t)$ is the overall~~
~~110 external sound pressure acting at the outer surface of the loudspeaker in Pa .~~
~~111 In the following, we will denote $C_{mc} = (1/C_{ms} + \rho c^2 S^2/V_b)^{-1}$ as the total~~
~~112 equivalent compliance of the enclosed loudspeaker. The electrical load can~~
~~113 be modeled by the following differential equation~~

$$e(t) = R_e i(t) + L_e \frac{di(t)}{dt} + Bl v_s(t) \quad (2)$$

~~114 with $e(t)$ the voltage applied at the electrical terminals. R_e and L_e are re-~~
~~115 spectively the DC resistance and the inductance of the voice coil and $Bl v_s(t)$~~
~~116 is the back electromotive force (EMF) induced by its motion through the~~
~~117 magnetic field. The Electrodynamic loudspeaker can be represented in the~~
~~118 form of an equivalent circuit including the electric load e as illustrated in~~
~~119 Figure 2.~~

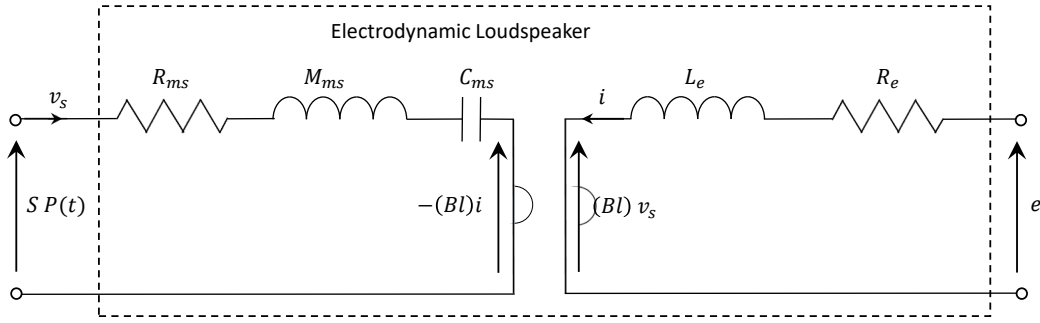


Figure 2: Circuit representation of an electrodynamic loudspeaker [8].

120 3. Electrical nonlinear shunt resistor

121 The use of nonlinearity in the form of an electrical circuit permits the
 122 existence of quasiperiodic regimes over a range of external forcing terms,
 123 which provide efficient vibration suppression [23]. Based on this assumption,
 124 and in order to design a nonlinear shunt resistor, we propose to connect an
 125 electric circuit enabling to obtain a pure cubic nonlinearity. As mentioned
 126 in [23] it is possible to obtain electronically a cubic nonlinearity using multi-
 127 pliers. Based on this concept, we propose to connect the following example
 128 of a nonlinear shunt circuit (see Figure 3, where the crossed boxes represent
 129 quadratic multipliers) to the transducer terminals.

130 One must mention that since we are connecting an unstable circuit, this
 131 kind of system becomes complicated to stabilize electronically. This is just an
 132 example of implementation; however, the practical realization may depend
 133 on weighting terms that will be considered as control parameters.

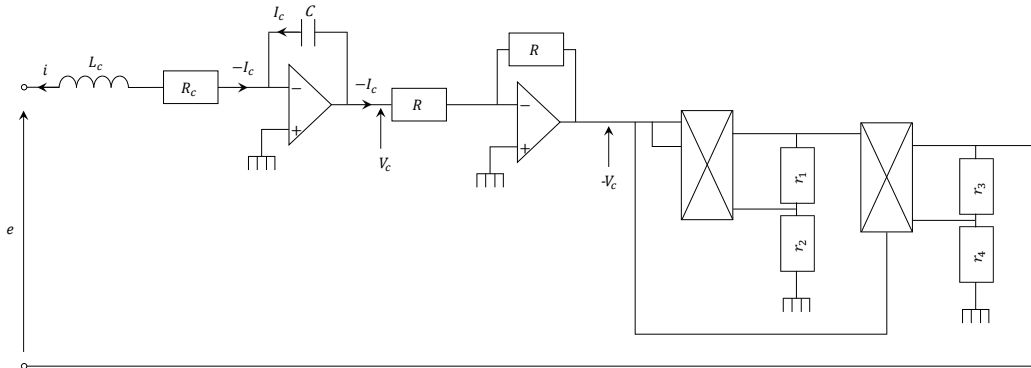


Figure 3: Nonlinear resonant circuit shunting.

134 The electrical nonlinear shunt circuit includes an inductor L_c , a resistor
 135 R_c playing the role of the NES linear damping coefficient and a capacitance
 136 C providing a pure cubic stiffness due the use of the multipliers. Then, the
 137 electrical voltage $e(t)$ can be expressed as follows

$$e(t) = -L_c \frac{di}{dt} - R_c i + V_c - V_c - kV_c^3 \quad (3)$$

138 where $k = k_1 k_2 \frac{(r_1 + r_2)(r_3 + r_4)}{r_1 r_2}$ is the nonlinear coefficient related to
 139 the multipliers connections with $1k\Omega \leq r_1, r_3$ and $r_2, r_4 \leq 100k\Omega$. The ratios
 140 k_1 and k_2 are homogeneous to the inverse of voltage (V^{-1}). Referring to the
 141 principle of operational amplifiers, the current I_C , through the capacitor C
 142 is given by

$$I_C = C \frac{dV_c}{dt} \quad (4)$$

143 Then, the driving current i can be expressed as follows

$$i(t) = -(-I_C) = C \frac{dV_c}{dt} \quad (5)$$

144 After replacing Equations (3,5) into Equations (1,2), the dynamics of the
 145 loudspeaker can be described by the following system of differential equations
 146 coupling the electrical and the mechanical parts

$$\begin{cases} M_{ms} \ddot{x}(t) + R_{ms} \dot{x}(t) + \frac{1}{C_{mc}} x(t) - CB_l \frac{dV_c}{dt} = SP(t) \\ C(L_e + L_c) \frac{d^2 V_c}{dt^2} + C(R_e + R_c) \frac{dV_c}{dt} + kV_c^3 + Bl \dot{x}(t) = 0 \end{cases} \quad (6)$$

147 Considering the fact that the front of the diaphragm is subjected to a
 148 periodically varying sound pressure $P(t) = A_m \cos(\omega t)$ with ω the angular
 149 frequency. $L_p = 20 \log_{10}(p/p_{\text{ref}})$ dB represents the sound pressure level with

150 $p = \sqrt{\frac{1}{T} \int_0^T P(t)^2 dt}$ the root mean square sound pressure and $P p_{\text{ref}} = 20$
 151 μPa is the reference sound pressure in the air.

152 From a global point of view, the circuit is not passive in the way that
 153 very few tenth of watt are used to power the amplifiers in the electronics.
 154 However, if we consider the electromechanical part on its own, the system is
 155 considered passive (negative energy dissipation) or semi-passive (the average

156 of the exchanged power is negative) enabling to determine the stability of
 157 the system. In the mechanical part, the pumped energy is dissipated by
 158 joule heating effect: we implement to dissipate. The aim of this paper is to
 159 show the effects of a new (passive) nonlinear control that is not necessarily
 160 optimized.

161 4. Analytical developments

162 An analytical treatment suitable for this kind of systems is detailed below.
 163 It allows to detect time multi-scale energy pumping between the primary
 164 system that describes the displacement of the loudspeaker and the shunt
 165 nonlinear circuit. This procedure can be divided into several steps: re-scaling,
 166 complexification of the system and keeping first harmonics and embedding
 167 time into fast and slow time scales. This schema permits the detection of
 168 the invariant manifold of the system at fast time scale, in addition to the
 169 equilibrium and fold singularities identification of the obtained reduced order
 170 system at slow time scales.

171 4.1. Rescaled system

172 For convenience and equation simplicity, we introduce the following non-
 173 dimensional variable $T = \omega_0 t$ with $\omega_0 = \sqrt{1/M_{ms}C_{mc}}$ representing the nat-
 174 ural frequency of the main system (Loudspeaker). Then, we write the linear
 175 and nonlinear coefficients with the following corresponding scaling with re-
 176 spect to realistic physical parameters where

$$\begin{cases} \frac{d}{dt} = \frac{d}{dT} \frac{dT}{dt} = \omega_0 \frac{d}{dT} \\ \frac{d^2}{dt^2} = \omega_0^2 \frac{d^2}{dT^2} \end{cases} \quad (7)$$

177 Then the system takes the following form

$$\begin{cases} \frac{d^2x}{dT^2} + R_{ms}C_{mc}\omega_0 \frac{dx}{dT} + x(T) - CB_lC_{mc}\omega_0 \frac{dV_c}{dT} = SA_mC_{mc} \cos\left(\frac{\omega}{\omega_0}T\right) \\ C\omega_0^2(L_e + L_c) \frac{d^2V_c}{dT^2} + C\omega_0(R_e + R_c) \frac{dV_c}{dT} + kV_c^3 + Bl\omega_0 \frac{dx}{dT} = 0 \end{cases} \quad (8)$$

178 In what follows, we will use the complexification method of Manevitch
 179 and the multiple scale approach to detect the system invariant manifold at

180 the fast time scale, and the system behavior at slower time scales. To do
 181 so, one must write the second equation of System (8) in a manner to have
 182 very small mass of the NES compared to the loudspeaker. According to
 183 the system physical parameters, the sum of inductance ($L_e + L_c$) is smaller
 184 than 1 H. Then, $\varepsilon = (L_e + L_c)/L_0$ with $L_0 = 1$ H can be considered as
 185 our small dimensionless parameter; describing the ratio of mass between the
 186 loudspeaker and the NES. Then, dividing the second equation by $C\omega_0^2 L_0$,
 187 System (8) can be written as

$$\begin{cases} \frac{d^2x}{dT^2} + R_{ms}C_{mc}\omega_0 \frac{dx}{dT} + x(T) - CBLC_{mc}\omega_0 \frac{dV_c}{dT} = SA_m C_{mc} \cos\left(\frac{\omega}{\omega_0}T\right) \\ \varepsilon \frac{d^2V_c}{dT^2} + \frac{(R_e + R_c)}{\omega_0 L_0} \frac{dV_c}{dT} + \frac{k}{C\omega_0^2 L_0} V_c^3 + \frac{Bl}{C\omega_0 L_0} \frac{dx}{dT} = 0 \end{cases} \quad (9)$$

188 The loudspeaker damping coefficient $R_{ms}C_{mc}\omega_0$ is smaller than one, so
 189 it can be expressed as $\varepsilon\lambda$. In addition, the NES damping coefficient $(R_e +$
 190 $R_c)/(\omega_0 L_0)$ can be expressed as $\varepsilon\gamma$ by choosing an appropriate control resistor
 191 R_c . Moreover, the coupling terms $CBLC_{mc}\omega_0$ and $Bl/(C\omega_0 L_0)$ can be written
 192 as $\varepsilon\alpha$ and $\varepsilon\eta$ respectively due primarily to the value of Bl and the chosen
 193 capacitance C . The value of the nonlinear cubic coefficient $k/(C\omega_0^2 L_0)$ can be
 194 adjusted by both k and C and then be expressed as $\varepsilon\xi$. On the other hand,
 195 the external forcing term $SA_m C_{mc}$ is of order 1, so it can be represented by
 196 εf

197 Then, the scaled differential system (9) becomes

$$\begin{cases} \frac{d^2x}{dT^2} + \varepsilon\lambda \frac{dx}{dT} + x(T) - \varepsilon\alpha \frac{dV_c}{dT} = \varepsilon f \cos\left(\frac{\omega}{\omega_0}T\right) \\ \varepsilon \left(\frac{d^2V_c}{dT^2} + \gamma \frac{dV_c}{dT} + \xi V_c^3 + \eta \frac{dx}{dT} \right) = 0 \end{cases} \quad (10)$$

198 In order to examine the damped nonlinear normal modes of system (10)
 199 in the vicinity of 1:1 resonance, both variables x and V_c are supposed to
 200 have frequency close to $\Omega = \omega/\omega_0$. The complex variables of Manevitch are
 201 introduced [24], which enable us to apply the truncated Fourier series later
 202 on ($i = \sqrt{-1}$):

$$\begin{cases} \frac{dx}{dT} + i\Omega x = \varphi_1 e^{i\Omega T} \\ \frac{dV_c}{dT} + i\Omega V_c = \varphi_2 e^{i\Omega T} \end{cases} \quad (11)$$

203 *4.2. Complexification-averaging procedure*

204 If the damped nonlinear normal modes for the case of 1:1 resonance is
 205 considered, then φ_1 and φ_2 which defines the coefficients of the Fourier series
 206 expansion of x and V_c may be considered as functions of slow time scales $\varepsilon^j T$
 207 ($j \geq 1$). In order to preserve only first harmonic $e^{i\Omega T}$ for each equation of
 208 System (10), we apply the Galerkin method and a truncated Fourier series.
 209 Then we obtain the following system

$$\begin{cases} \dot{\varphi}_1 - i\frac{(1-\Omega^2)}{2\Omega}\varphi_1 + \varepsilon\frac{\lambda}{2}\varphi_1 - \varepsilon\frac{\alpha}{2}\varphi_2 = \varepsilon\frac{1}{2}f \\ \varepsilon\left[\dot{\varphi}_2 + i\frac{\Omega}{2}\varphi_2 + \frac{\gamma}{2}\varphi_2 - i\frac{\xi}{2\Omega}\varphi_2 G(|\varphi_2|^2) + \frac{\eta}{2}\varphi_1\right] = 0 \end{cases} \quad (12)$$

210 with $G(|\varphi_2|^2) = \frac{3}{4\Omega^2}|\varphi_2|^2$ representing the resonant term.

211 *4.3. Multiple-scale analysis*

212 System (12) may be analyzed by using a multiple time scales approach,
 213 where we introduce the slow times τ_1, τ_2, \dots and the fast time τ_0 as

$$\tau_0 = T \quad \tau_j = \varepsilon^j T \quad j = 1, 2, \dots \quad (13)$$

214 so that

$$\frac{d}{dT} = \frac{\partial}{\partial\tau_0} + \varepsilon\frac{\partial}{\partial\tau_1} + \varepsilon^2\frac{\partial}{\partial\tau_2} + \dots \quad (14)$$

215 We will analyze the system behavior around 1:1 resonance by using a
 216 multiple scales approach assuming that

$$\Omega = 1 + \varepsilon\sigma \quad (15)$$

217 with σ a detuning parameter. At the order ε^0 , resonant terms at τ_0 scale
 218 in system (12) yields

$$\frac{\partial \varphi_1}{\partial \tau_0} = 0 \Rightarrow \varphi_1 = \varphi_1(\tau_1, \tau_2, \dots) \quad (16)$$

219 The previous equation shows that the function φ_1 is constant during the
 220 time $\tau_0 = T$, which means that in the principal approximation φ_1 depends
 221 on the slow times τ_1, τ_2, \dots . However, at the order ε^1 the first equation of
 222 system (12) gives

$$\begin{cases} \frac{\partial \varphi_1}{\partial \tau_1} + i\sigma\varphi_1 + \frac{\lambda}{2}\varphi_1 - \frac{\alpha}{2}\varphi_2 = \frac{1}{2}f \\ \frac{\partial \varphi_2}{\partial \tau_0} + i\frac{1}{2}\varphi_2 + \frac{\gamma}{2}\varphi_2 + \frac{\eta}{2}\varphi_1 - i\frac{\xi}{2}\varphi_2 G(|\varphi_2|^2) = 0 \end{cases} \quad (17)$$

223 Fixed points corresponds to the behavior of φ_2 for $\tau_0 \rightarrow +\infty$ which means
 224 $\frac{\partial \varphi_2}{\partial \tau_0} = 0$ can be obtained from Equation (18):

$$[\gamma + i(1 - \xi G(|\varphi_2|^2))]\varphi_2 = -\eta\varphi_1. \quad (19)$$

225 Equation (19) presents an asymptotic equilibrium governed by a manifold
 226 called Slow Invariant Manifold (SIM). By writing φ_1 and φ_2 into their polar
 227 form as $\varphi_1 = N_1 e^{i\delta_1}$ and $\varphi_2 = N_2 e^{i\delta_2}$, Equation (19) can be written and
 228 reduced into the following form:

$$\eta N_1 e^{i(\delta_1 - \delta_2)} = -iN_2 - \gamma N_2 + i\xi N_2 G(N_2^2). \quad (20)$$

229 Taking into account the definitions of the complex variables φ_1 and φ_2 ,
 230 their modules N_1 and N_2 can be expressed in terms of the initial variables x
 231 and V_c of the physical system as

$$\begin{cases} N_1 = |\varphi_1| = \sqrt{\left(\frac{dx}{dT}\right)^2 + \Omega^2 x^2} \\ N_2 = |\varphi_2| = \sqrt{\left(\frac{dV_c}{dT}\right)^2 + \Omega^2 V_c^2} \end{cases} \quad (21)$$

232 After separating the real and imaginary parts of Equation (20), one can
 233 reach the following system

$$\begin{cases} \gamma N_2 = -\eta N_1 \cos(\delta_1 - \delta_2), \\ (1 - \xi G(N_2^2))N_2 = -\eta N_1 \sin(\delta_1 - \delta_2). \end{cases} \quad (22)$$

$$\begin{cases} \gamma N_2 = -\eta N_1 \cos(\delta_1 - \delta_2), \\ (1 - \xi G(N_2^2))N_2 = -\eta N_1 \sin(\delta_1 - \delta_2). \end{cases} \quad (23)$$

234 Taking the square of both sides of equations (22) and (23) and summing
 235 them, we obtain

$$N_1 = \frac{N_2}{\eta} \sqrt{\gamma^2 + (1 - \xi G(N_2^2))^2}. \quad (24)$$

236 Local extrema of Equation (24) can be revealed using the following criteria

$$\frac{\partial N_1^2}{\partial N_2^2} = 0, \quad (25)$$

237 which finally yields the equation

$$\gamma^2 + (1 - \xi G(N_2^2))(1 - \xi G(N_2^2) - 2\xi N_2^2 G'(N_2^2)) = 0. \quad (26)$$

238 Equation (26) can be verified when the damping coefficient γ associated
 239 to the nonlinear equation is smaller than a critical value γ_c which is equal
 240 to $1/\sqrt{3}$ [23]. In addition, depending on the value of γ the system can have
 241 one, two or three fixed points. Moreover, for $\gamma < \gamma_c$ there exists two local
 242 extrema called N_{21} and N_{22} that can be written as follows

$$N_{21} = \frac{2}{3} \sqrt{\frac{2}{\xi} - \frac{\sqrt{1 - 3\gamma^2}}{\xi}}, \quad N_{22} = \frac{2}{3} \sqrt{\frac{2}{\xi} + \frac{\sqrt{1 - 3\gamma^2}}{\xi}}. \quad (27)$$

243 It has been proved that the stable area of the fixed points in the reduced
 244 linearized system at the τ_0 time scale can be defined by the following criterion
 245 [25]

$$\gamma^2 + (1 - \xi G(N_2^2))(1 - \xi G(N_2^2) - 2\xi N_2^2 G'(N_2^2)) \geq 0 \quad (28)$$

246 According to the previous inequality, stable fixed points corresponds to
 247 $N_2 < N_{21}$ and $N_2 > N_{22}$. By substituting the stable solution φ_2 with respect
 248 to the fast time scale τ_0 generated in Equation (19) into Equation (17),
 249 writing φ_2 into its polar form as $\varphi_2 = N_2(\tau_1)e^{i\delta_2(\tau_1)}$ and separating the real
 250 and imaginary parts of the resulting equation one finally obtains the following
 251 system

$$\begin{cases} \frac{\partial N_2}{\partial \tau_1} = \frac{\mathbf{BF} - \mathbf{DE}}{\mathbf{AD} - \mathbf{CB}} = \frac{f_1(N_2, \delta_2)}{g(N_2)}, \\ \frac{\partial \delta_2}{\partial \tau_1} = \frac{\mathbf{CE} - \mathbf{AF}}{\mathbf{AD} - \mathbf{CB}} = \frac{f_2(N_2, \delta_2)}{g(N_2)}. \end{cases} \quad (29)$$

252 Explicit values of \mathbf{A} , \mathbf{B} , \mathbf{C} , \mathbf{D} , \mathbf{E} and \mathbf{F} are given in Appendix A. The
 253 approximation of the fast time scale τ_0 , enables Equations (17,18) to illustrate
 254 the response of the system regarding the initial conditions, when the system
 255 approaches the resonance manifold. In addition, the approximation of N_2
 256 and δ_2 represented by System (29), describes the slow-time τ_1 evolution of
 257 the system at the manifold.

258 Equilibrium points of the system are defined by $f_1(N_2, \delta_2) = f_2(N_2, \delta_2) =$
 259 0 and $g(N_2) \neq 0$ while fold singularities are given by $f_1(N_2, \delta_2) = f_2(N_2, \delta_2) =$
 260 $g(N_2) = 0$. We should note that the stability of $g(N_2)$ can be treated as same
 261 as the invariant manifold (see Equation (24)). In fact, $g(N_2) = 0$ provides
 262 both extrema N_{21} and N_{22} which are called the fold lines of the system.

263 5. Observation of free oscillations

264 In order to illustrate the mechanism of Targeted Energy Transfer (TET)
 265 between the primary system and the NES according to the slow time τ_1 , we
 266 start by setting $Z_1 = N_1^2$ and $Z_2 = N_2^2$. Hence, in the case of free oscillations
 267 and by using the first equation of System (29), $\partial Z_2 / \partial \tau_1$ can be written in
 268 the following form

$$\frac{\partial Z_2}{\partial \tau_1} = - \frac{\alpha\gamma\eta + \lambda \left(\gamma^2 + (1 - \xi G(Z_2))^2 \right)}{\gamma^2 + (1 - \xi G(Z_2)) (1 - 2Z_2 \xi G'(Z_2) - \xi G(Z_2))} Z_2. \quad (30)$$

269 The integral of the previous equation can be computed explicitly as below

$$\mathcal{R}(\tau_1, Z_2) = Cte \quad (31)$$

270 with

$$\begin{aligned}
\mathcal{R}(\tau_1, Z_2) = & 2\lambda\sqrt{\alpha\eta + \gamma\lambda}(\alpha\gamma\eta + \lambda + \gamma^2\lambda)\tau_1 + \left[2\alpha\eta\sqrt{\gamma\lambda} \arctan \left[\right. \right. \\
& \left. \left. \sqrt{\frac{\lambda}{\gamma(\alpha\eta + \gamma\lambda)}\left(1 - \frac{3}{4}\xi Z_2\right)} \right] + \sqrt{\alpha\eta + \gamma\lambda} \left(2(1 + \gamma^2)\lambda \log(Z_2) \right. \right. \\
& \left. \left. + \left(3\alpha\gamma\eta + 2(1 + \gamma^2)\lambda \right) \log \left[16\alpha\gamma\eta + \lambda(16\gamma^2 + (4 - 3\xi Z_2)^2) \right] \right) \right] \quad (32)
\end{aligned}$$

271 and *Cte* is an integration constant that can be related to the initial con-
272 ditions. In fact, Z_1 and Z_2 reflect the energy stored in the relative displace-
273 ment of the loudspeaker membrane and the voltage across the capacitor in
274 the nonlinear shunt circuit respectively.

275 6. Results and discussions

276 6.1. Validation of the approach

277 In order to validate the obtained analytical approaches, we use a direct nu-
278 merical integration method. The function `ode45` implemented in MATLAB©
279 which is based on an explicit Runge-Kutta (4,5) formula is employed in order
280 to solve the dimensional differential system (10) and the complex averaged
281 one (12).

282 We consider the scaled parameters: $\varepsilon = 0.01$, $\lambda = 0.1$, $\alpha = 0.1$, $\gamma = 0.35$,
283 $\eta = 0.1$ and $\xi = 0.5$ and the following initial conditions: $x(0) = V_c(0) =$
284 $V_c(0) = 0$ and $\dot{x}(0) = 7$. For free oscillations ($f = 0$), Figure 4 shows a
285 comparison of N_1 and N_2 between numerical solutions obtained by direct
286 integration of the initial differential system (10) and the averaged one (12).
287 Curves shown in Figure 4 includes three various phenomena stages [26]. The
288 first one begins from the initial point of the simulation until almost $\tau_0 = 550$,
289 where the NES maximal amplitude decreases slowly and the main system
290 decreases rapidly. In the second stage and around $\tau_0 = 550$, the system
291 reaches a local extrema during which N_2 decreases abruptly and N_1 is al-
292 most constant. Finally, during the third stage ($\tau_0 > 550$) both amplitudes
293 decreases almost linearly. Since the numerical results of the very first differ-
294 ential system (12) includes all harmonics, when we kept the first harmonic
295 and truncated the highest ones for the averaged system (10), we can remark
296 the good agreement between both results.

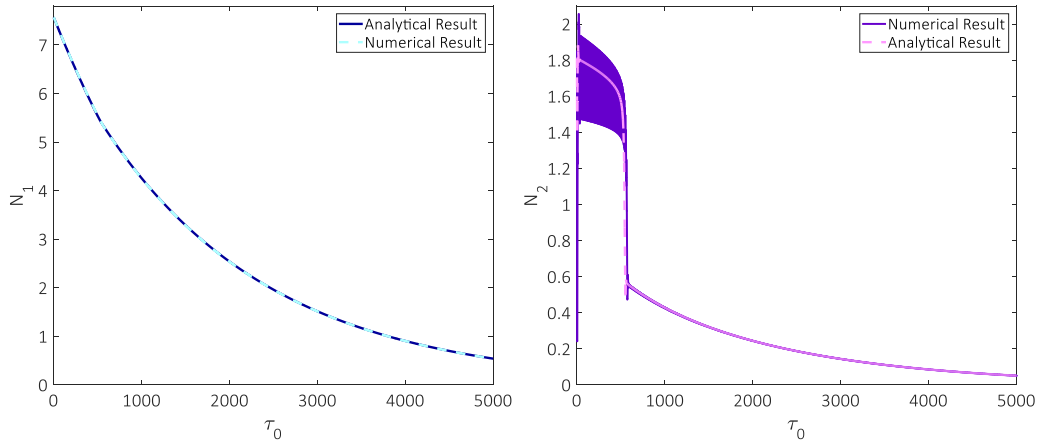


Figure 4: Numerical and analytical results for N_1 and N_2 during free vibrations.

297 At τ_0 time scales, fixed points of the system are represented by the Slow
 298 Invariant Manifold (SIM) shown in Figure 5. Full and dashed lines corre-
 299 spond to stable and unstable parts of the τ_0 invariant respectively with N_{21}
 300 and N_{22} defining the extrema according to the N_2 variable. In fact, the SIM
 301 corresponds to a geometrical representation of all types of system behaviors
 302 in the slow time scales regardless the forcing term. In the following sections,
 303 we will provide a detailed study about the different dynamics of the system
 304 during free and forced vibrations.

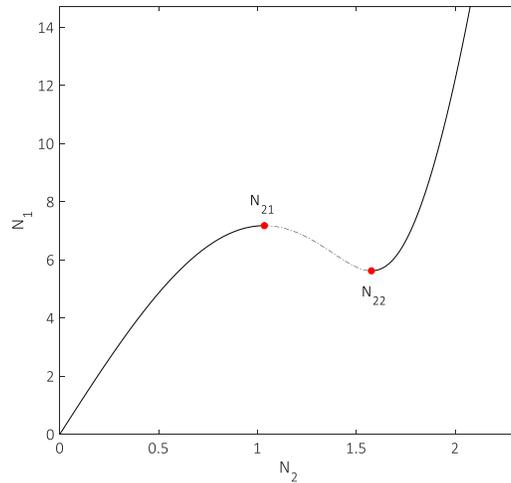


Figure 5: τ_0 invariant where stable and unstable parts are represented in full and dashed lines respectively. N_{21} and N_{22} define the extrema according to the N_2 variable.

305 For free oscillations, the analytical energy trends can be obtained by solv-
 306 ing Equation (31) with a corresponding constant C , providing an illustration
 307 of the possible scenarios of TET according to the initial conditions [27].

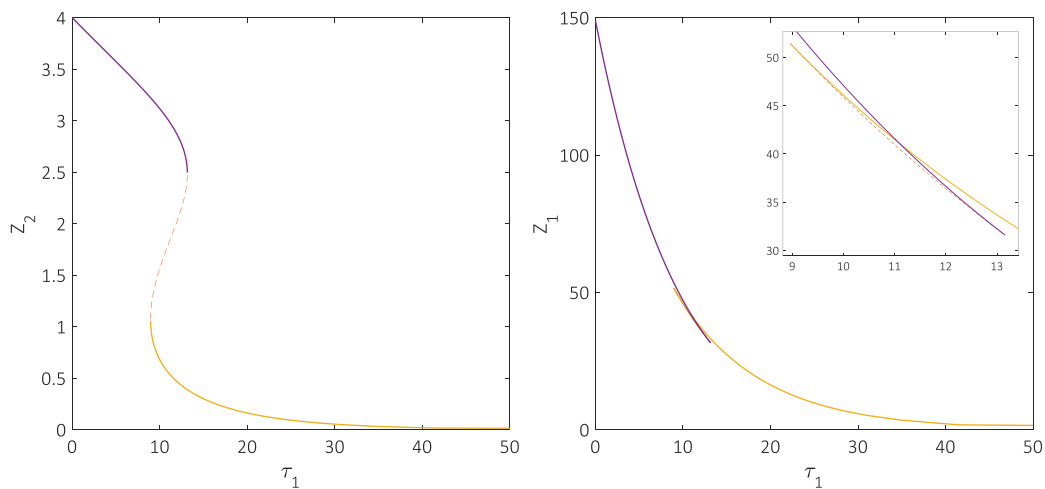


Figure 6: Analytical energy trends obtained by solving Equation (31) for a corresponding constant C .

308 Figure 6 shows that two stable possibilities of energy pumping for the
 309 cases of free oscillations can be reached. More precisely, for initial conditions
 310 corresponding to a fixed point on the lower branch of the SIM, the mechanism
 311 of energy shows that this case is not efficient for TET. However, for initial
 312 conditions corresponding to a fixed point on the upper branch of the SIM,
 313 Figure 7 demonstrate that the process of energy is favorable for optimal NES
 314 design. It can be concluded that in order to activate the NES for efficient
 315 TET, initial conditions must be chosen in a manner that $N_1(0)$ is greater
 316 than the maximum N_{21} ordinate.

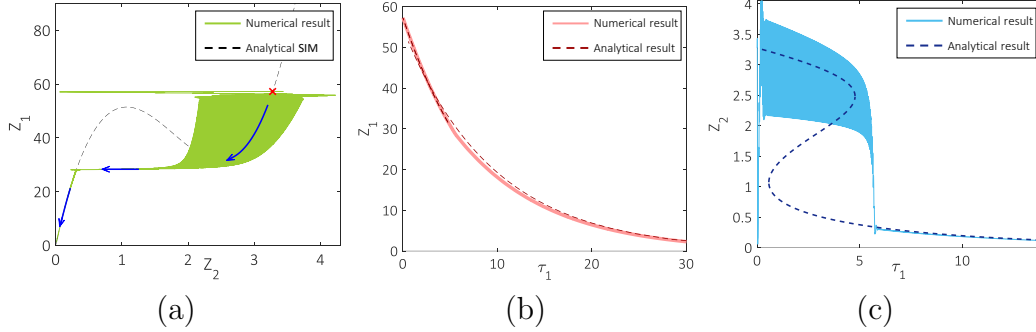


Figure 7: (a) Efficient passive TET to the NES for the case of free oscillations with initial conditions corresponding to a fixed point on the upper branch of the SIM. (b) and (c) show a comparison of energy flow between the numerical integration of the initial differential System (10) in full lines and the analytical results obtained by solving Equation (31) in dashed lines.

317 *6.2. Application*

318 In order to study the system behavior when coupling a nonlinear shunt
 319 resonator, we consider the physical parameters as Lissek et al. [8] from the
 320 electrodynamic moving coil to the enclosure volume which are listed in Table
 321 1.

Table 1: Visaton al 170 electrodynamic moving coil loudspeaker parameters

Parameter	Symbol	Value	Unit
DC resistance	R_e	5.6	Ω
Voice coil inductance	L_e	0.9	mH
Force factor	Bl	6.9	NA^{-1}
Moving mass	M_{ms}	13	g
Mechanical resistance	R_{ms}	0.8	Nm^{-1}s
Mechanical compliance	C_{ms}	1.2	mmN^{-1}
Effective area	S	133	cm^2
Sound celerity in the air	c	343	ms^{-1}
Enclosure volume	V_b	10	dm^3
Air density	ρ	1.18	Kg m^{-3}

322 Among the large set of physical parameters that can be considered in
 323 the nonlinear shunt circuit, additional criteria are required. For instance,
 324 according to our choice of scaling and since the NES damping constant γ

325 must be smaller than $1/\sqrt{3}$ as detailed previously, the choice of the control
 326 resistor R_c must verify the following inequality

$$0 < R_c + R_e < \varepsilon \frac{\omega_0}{\sqrt{3}}. \quad (33)$$

327 Initial conditions were considered in a manner that the loudspeaker mem-
 328 brane is subjected to an initial velocity $\dot{x}(0) \neq 0$. The rest of the initial con-
 329 ditions are assumed to be null: $x(0) = V_c(0) = \dot{V}_c(0) = 0$, which corresponds
 330 to $N_2(0) = 0$ and $N_2(0) = N_0 = \dot{x}(0)$. N_0 is chosen in a manner to be above
 331 the ordinate of the SIM maximum ($N_0 > N_{11}$) to examine a situation where
 332 the NES is active to control oscillations. Then, we set the control parameters
 333 of the nonlinear electric shunt in Table 2.

Table 2: Configuration presenting the operational amplifiers parameters

Parameter	Resistance R_c (Ω)	Inductance L_c (mH)	Capacitance C (mF)	Nonlinear coefficient k (V^{-2})
Test 1	1	50	5	8160
Test 2	-4.7	5	5	8160

334 6.3. Results for parameters of Test 1

335 In what follows, we will study the system behaviors for the physical pa-
 336 rameters listed in Table 2 untitled Test 1 for and forced oscillations.

337 6.3.1. Free oscillations

338 Figure 8 shows N_1 vs N_2 , with a comparison between the analytical invari-
 339 ant manifold given in Equation (24) (dashed-dotted curve) and the numerical
 340 integration of the differential system (10) (full line). Remarkably, the behav-
 341 ior of the system amplitudes N_1 and N_2 tracks the SIM. More precisely, full
 342 curve undergoes an immediate jump and oscillates around the lower stable
 343 branch until its amplitude decreases quasi-linearly.

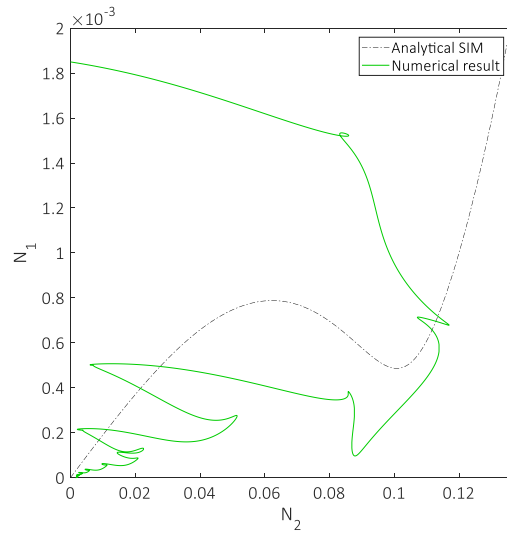


Figure 8: Invariant manifold of the system at the fast time scale τ_0 (black curve) and its corresponding numerical results (green curve) for the system under free oscillations $P(t) = 0$ and $\sigma = 0$. Numerical results correspond to the integration of System (10) versus t for $t \in [0, 0.15]$ with the initial conditions $x(0) = V_c = \dot{V}_c = 0$ and $\dot{x}(0) = 1.9 \times 10^{-3} \text{ m s}^{-1}$.

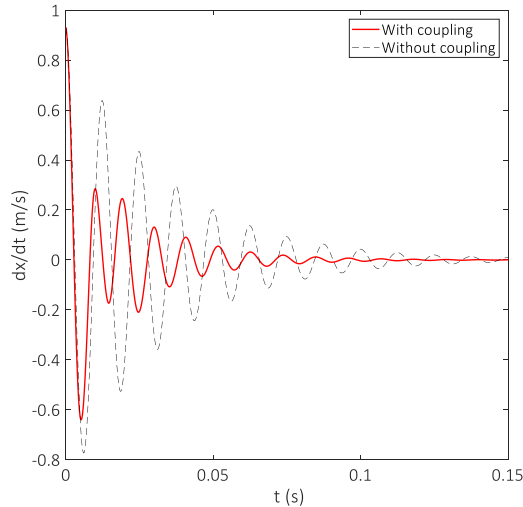


Figure 9: Histories of displacement in terms of time $t(s)$ obtained by numerical integration of the system under free vibrations, $\sigma = 0$ with the initial conditions corresponding to $x(0) = V_c = \dot{V}_c = 0$ and $\dot{x}(0) = 1.9 \times 10^{-3} \text{ m s}^{-1}$. Dashed and full lines denote the cases of open circuit and shunt nonlinear circuit respectively.

344 In fact, when choosing initial conditions that corresponds to a point above
 345 N_{21} , energy flows immediately and encounters a sudden breakdown toward
 346 the stable lower branch. In other words, the energy in the loudspeaker mem-
 347 brane is irreversibly streamed toward the nonlinear shunt circuit until it
 348 converges to zero.

349 The corresponding velocity histories versus time are represented in full
 350 line in Figure 9. Dashed curve represents the velocity histories in terms
 351 of time for the case of open circuit, which means when the electroacoustic
 352 transducer is not coupled with any electric charge. Clearly, the NES permits
 353 reduction of oscillations amplitudes.

354 6.3.2. Primary system under external forcing

355 Unlike the previous investigations, the loudspeaker diaphragm is now sub-
 356 jected to a periodically varying sound pressure $P(t)$. As detailed previously,
 357 at the slow time scale τ_1 , all achievable system dynamics can be obtained by
 358 solving (29). More precisely, equilibrium points which corresponds to peri-
 359 odic regimes are obtained when $f_1(\delta_2, N_2) = f_2(\delta_2, N_2) = 0$ and $g(N_2) \neq 0$,
 360 where fold singularities corresponds to quasi-periodic regimes are achievable
 361 when $f_1(\delta_2, N_2) = f_2(\delta_2, N_2) = g(N_2) = 0$.

362 As the scaled forcing term f is proportional to the pressure amplitude A_m
 363 which is defined as a function of the sound pressure level L_p , this later is con-
 364 sidered as a main parameter of the nonlinear study. For instance, considering
 365 $\sigma = 0$ which corresponds to the resonance frequency ω_0 , Figure 10 represent
 366 the cartography of the achievable dynamics of the system for several values
 367 of sound pressure levels (L_p). Horizontal dashed black lines define the sta-
 368 bility boundaries N_{21} and N_{22} . dash-dotted and full line curves correspond
 369 respectively to $f_1(\delta_2, N_2) = 0$ and $f_2(\delta_2, N_2) = 0$. According to the value of
 370 L_p , the positions and the number of fold singularities and equilibrium points
 371 change so as their stability. More precisely, when full line and dash-dotted
 372 curves intersect each other far from the fold lines in black (N_{21}, N_{22}) we can
 373 deduce the existence of an equilibrium points which corresponds to a peri-
 374 odic regime. Otherwise, when they intersect on a fold line, fold singularities
 375 corresponding to quasi-periodic regime can be identified.

376 The color shade together with the numbers from 1 to 6 correspond to
 377 the pressure levels $L_p = \{116, 120, 124, 128, 132, 136\}$ (dB) respectively. The
 378 stars and the triangle illustrate the positions of equilibrium points for each
 379 L_p and the dots denote fold singularities corresponding to $L_p = 132$ dB.

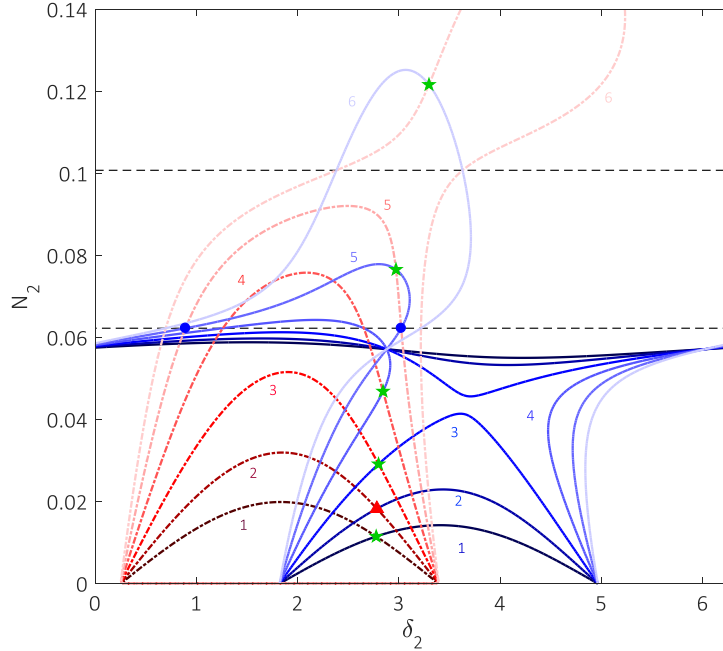


Figure 10: Positions of equilibrium points marked with stars for the system under several values of sound pressure levels $L_p = \{116, 120, 124, 128, 132, 136\}$ (dB) for the detuning parameter $\sigma = 0$. $g(N_2) = 0$ corresponds to the dotted horizontal black lines N_{21} and N_{22} . $f_1(\delta_2, N_2) = 0$ and $f_2(\delta_2, N_2) = 0$ are represented in dash-dotted and full line curves respectively.

380 For $L_p = 120$ dB and $\sigma = 0$, Figure 10 shows the existence of one equi-
381 librium point represented in triangle, corresponding to the intersection of
382 full line and dash-dotted curves labeled 2 far the fold singularities. Fig-
383 ure 11 shows the evolution of numerical values $N_1 = |dx/dT + i\Omega x|$, $N_2 =$
384 $|dV_C/dT + i\Omega V_c|$ (Green curve) obtained by numerical integration of System
385 (10) compared to the invariant manifold. We can see that the system oscil-
386 lates around the lower stable branch of the invariant until being attracted
387 by the fixed point. The corresponding velocity time series is represented in
388 Figure 12, where we compare the histories of $\dot{x}(t)$ with and without coupling
389 in addition to the time histories of $\dot{V}_c(t)$. The periodic regimes obtained
390 numerically validate our analytical predictions illustrated by the equilibrium
391 point in Figure 10. In fact, the energy was transmitted from the loudspeaker
392 membrane under periodic sound pressure to the non-excited nonlinear shunt
393 circuit, with the same frequency defining the 1:1 resonance.

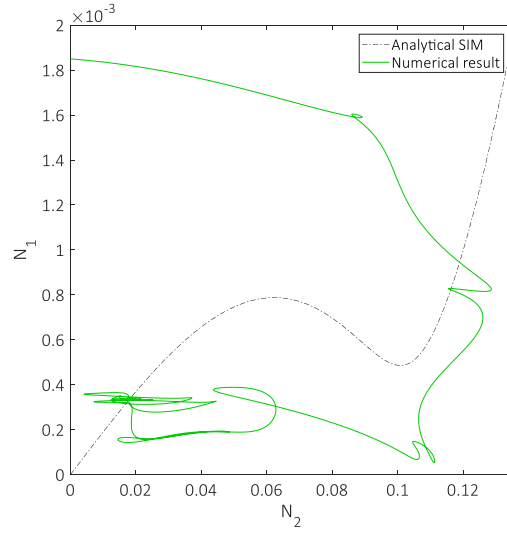


Figure 11: System invariant manifold and its corresponding numerical result for $L_p = 120$ dB and $\sigma = 0$. The numerical result corresponds to the integration of System (10) with the initial conditions corresponding to $x(0) = V_c = \dot{V}_c = 0$ and $\dot{x}(0) = 1.9 \times 10^{-3} \text{ m s}^{-1}$. In this case, the system is attracted by the periodic regime that corresponds to the fixed point marked with a triangle in Figure 10.

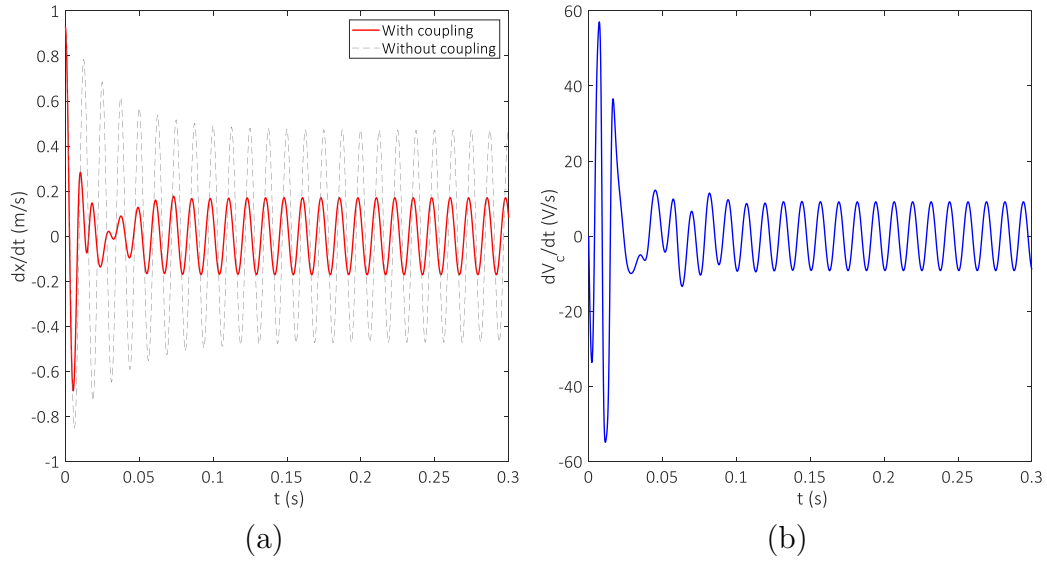


Figure 12: (a) Comparison of velocity histories as a function of time t (s) obtained by numerical integration of the system under $L_p = 120$ dB between the master system (The loudspeaker) coupled with the NES (the shunt nonlinear circuit) represented in solid lines and without the NES in dotted line. (b) Histories of the voltage derivative in terms of time t (s).

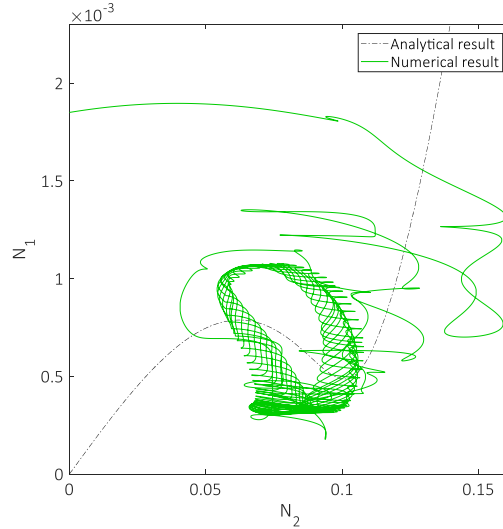


Figure 13: System invariant manifold and its corresponding numerical result for $L_p = 132$ dB and $\sigma = 0$. The numerical result corresponds to the integration of System (10) with the initial conditions corresponding to $x(0) = V_c = \dot{V}_c = 0$ and $\dot{x}(0) = 1.9 \times 10^{-3} \text{ m s}^{-1}$. Here, the system present a SMR illustrated in Figure 10 with two dots.

394 For $L_p = 132$ dB and $\sigma = 0$, we can deduce from the dash-dotted and
 395 solid curves labeled 5 in Figure 10 that the system possesses one unsta-
 396 ble equilibrium point marked with a stars between the fold lines and two
 397 fold singularities denoted by dots. Hence, the corresponding numerical re-
 398 sult and the analytical invariant are shown in Figure 13. This curve refers
 399 to a Strongly Modulated Response (SMR) of the system, including jump
 400 phenomena between both fold lines. In fact, for similar behavior both the
 401 loudspeaker membrane and the nonlinear shunt circuit are beating, which
 402 is very favorable for passive energy harvesting control applications. Energy
 403 exchange process of the SMR is qualitatively well described by the jump
 404 phenomenon in Figure 13. Besides, the values of N_2 seem to be perfectly ap-
 405 propriate when the jumps occur. However, some quantitative errors appear
 406 for the values of N_1 due to several factors. Among them we can mention the
 407 choice of ε , the numerical inaccuracies besides the choice of the Manevitch
 408 complex variables which takes into account the first harmonic only.

409 Figure 14 shows the corresponding numerical results using a Runge-Kutta
 410 schema according to the time $t \in [0, 0.6]$. In addition, Figure 15 shows
 411 the Poincaré's section after eliminating the data corresponding to the tran-
 412 sient regime of both primary structure and attached nonlinear circuit. These

413 figures confirm the obtained quasi-periodic regime. In fact, an important
 414 amount of vibrational energy is rapidly transferred to the NES and damped
 415 out in a quasi-periodic regime. Thus, the attenuation of vibrational energy
 416 of the loudspeaker arise with good efficiency in the vicinity of the natural
 417 frequency ω_0 .

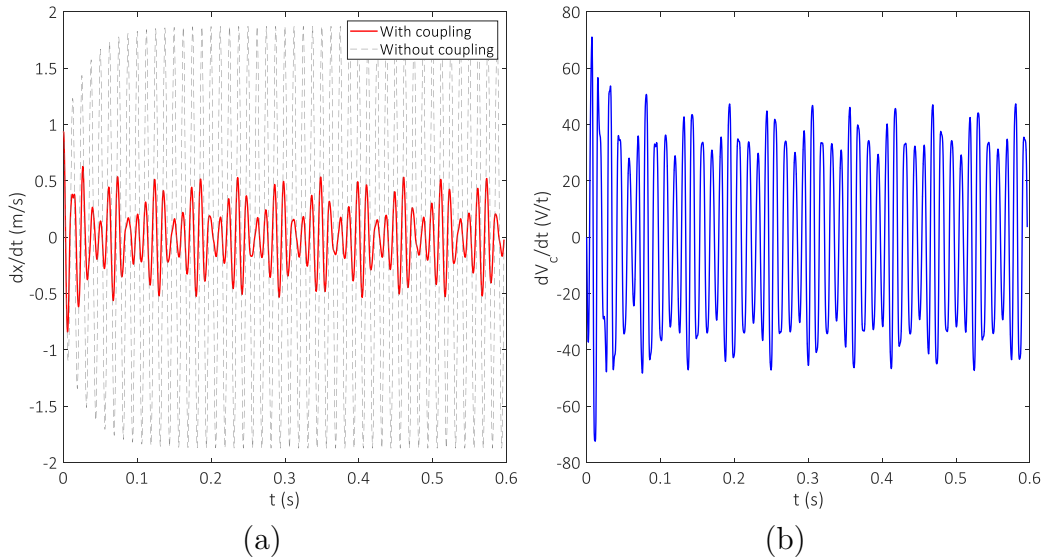


Figure 14: (a) Comparison of velocity histories as a function of time t (s) obtained by numerical integration of the system under $L_p = 132$ dB between the master system (The loudspeaker) coupled with the NES (the shunt nonlinear circuit) represented in solid line and without NES in dotted line. (b) Histories of the voltage derivative in terms of time t (s).

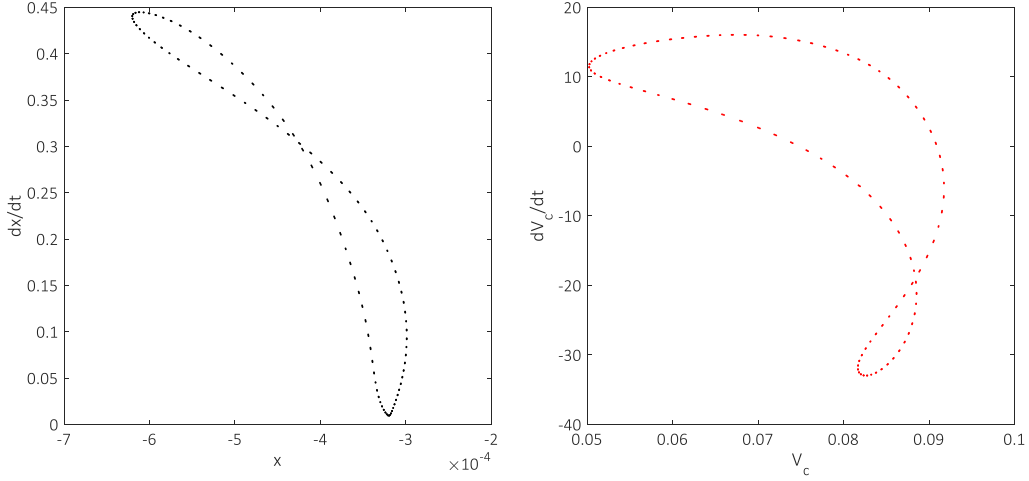


Figure 15: Poincaré’s section of the primary structure (Shunted loudspeaker) and the NES (nonlinear eclectic shunt circuit) showing a quasi-periodic vibrational regime.

418 *6.4. Results for parameters of Test 2*

419 For the set of physical parameters untitled Test 2 listed in Table 2, we
 420 study the system behavior for two different levels of sound pressure. **Al-**
 421 **though, a negative impedance converter circuit is needed to correctly use a**
 422 **negative value of control resistor R_c , Figure 3 represents an analog circuit**
 423 **that does not necessarily represent the real physical implementation. Besides,**
 424 **The negative test value is employed to compensate the positive resistance of**
 425 **the coil R_e and reach a point of optimality.**

426 For $\sigma = 0$, Figure 16 (a) and (b) show respectively the system invariant
 427 manifold (black curve) compared to the corresponding numerical integration
 428 of System (10) for $L_p = 115$ dB and $L_p = 124$ dB respectively, in addition
 429 to the corresponding histories of velocity. The initial conditions correspond
 430 to $x(0) = V_c = \dot{V}_c = 0$ and $\dot{x}(0) = 4 \times 10^{-5}$ m s⁻¹. Two different regimes
 431 can be identified: a periodic regime for the sound pressure level $L_p = 115$
 432 dB and a quasi-periodic one for $L_p = 124$ dB. Remarkably, for the present
 433 set of physical parameters (Test 2), we attenuate with a lower amplitude the
 434 membrane velocity.

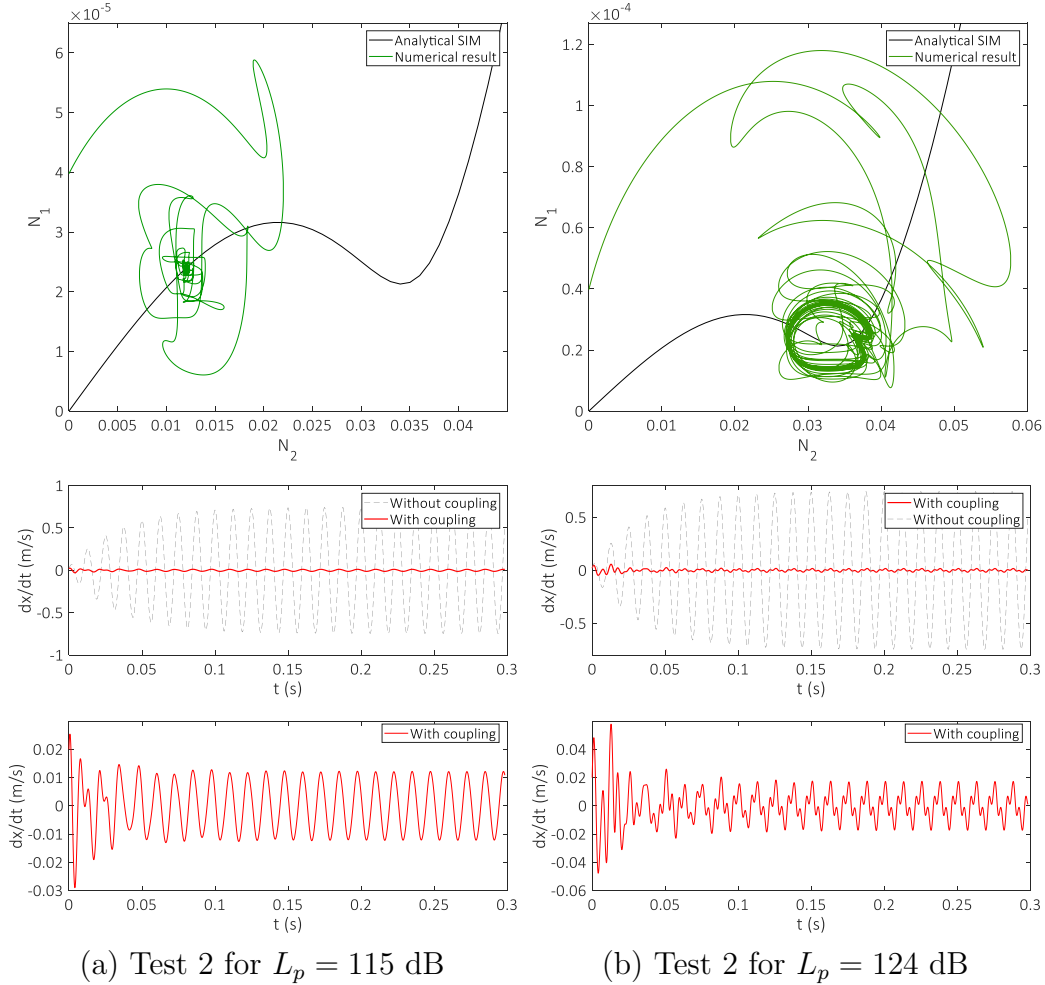


Figure 16: (a) and (b) show the results for test 2 for for $L_p = 115$ dB and for $L_p = 124$ dB respectively. Upper figures represent the system manifold invariant and their corresponding numerical results with $\sigma = 0$. The numerical results correspond to the integration of System (10) with the initial conditions corresponding to $x(0) = V_c = \dot{V}_c = 0$ and $\dot{x}(0) = 4 \times 10^{-5} \text{ m s}^{-1}$. The middle and lower figures show the comparison of velocity histories as a function of time $t(\text{s})$ obtained by numerical integration of the studied system without coupling (black dotted line) and with nonlinear coupling (red solid line). Here, the system present a periodic regime for (a) and a SMR illustrated for (b).

6.4.1. Acoustic admittance

In order to examine the influence of coupling a passive nonlinear shunt circuit to the transducers terminals, it is necessary to have an understanding of the sound wave propagation. The normalized acoustic admittance presented

439 at the loudspeaker diaphragm provides information about the amplitude of
 440 the reflection for a given frequency, which can be written as follows

$$Y_m(\omega) = -\rho c \frac{V(\omega)}{P_t(\omega)}, \quad (34)$$

441 with $V(w)$ and $P_t(w)$ are the Fourier transforms of $v(t)$ and $p_t(t)$ respec-
 442 tively. The minus sign appears as $V(w)$ is defined to describe the outgoing
 443 diaphragm velocity.

444 According to the previous analytical investigations detailed in Section
 445 6.3.2 at the τ_1 time scale and for the case of 1:1 resonance, two different
 446 regimes can be distinguished. The periodic or the quasi-periodic regimes
 447 are reached according to the given values of the forcing term and frequency.
 448 Then, in order to represent the obtained normalized admittance for a given
 449 sound pressure level we followed the process below.

450 For each ω in the frequency domain we integrate the differential system
 451 using an explicit Runge-Kutta (4,5) algorithm implemented in Matlab© from
 452 $t_0 = 0$ to $t_f = NT$ (N denoting the number of periods $T = 2\pi/\omega$) with
 453 $y_0 = [0, 0, 0, 0]$ as initial conditions.

454 Then, in the permanent regime, a study of Poincaré section has been
 455 applied. More precisely, we calculate the value of $\Delta(P^m) = |P^{m+1}(\dot{x}) -$
 456 $P^m(\dot{x})|$ for a certain number M of periods, where $P^m(\dot{x})$ corresponds to the
 457 intersection of the trajectory $\dot{x}(\dot{x}_0, t_0; t)$ with the plane $t = t_0 + mT$ with
 458 \dot{x}_0 is an initial velocity at time $t = t_0$ and $m \in 1, 2, \dots, M$. In the case
 459 when $\Delta(P^m)$ converges to zero in the stationary regime, a periodic regime
 460 can be identified. Therefore, the membrane velocity $\dot{x}(t)$ can be expressed as
 461 a Fourier series in the following form

$$\dot{x}(t) = a_0 + \sum_{n=1}^{\infty} (a_n \cos(n\omega t) + b_n \sin(n\omega t)), \quad (35)$$

462 and the normalized admittance is then represented by its \mathbf{L}_2 -norm which
 463 corresponds to $(\rho c/A_m) \sqrt{\sum_n (a_n^2 + b_n^2)}$. Otherwise, a quasi-periodic regime
 464 occurs and so the velocity is chosen to be represented by the absolute value
 465 of the peaks maximum amplitude.

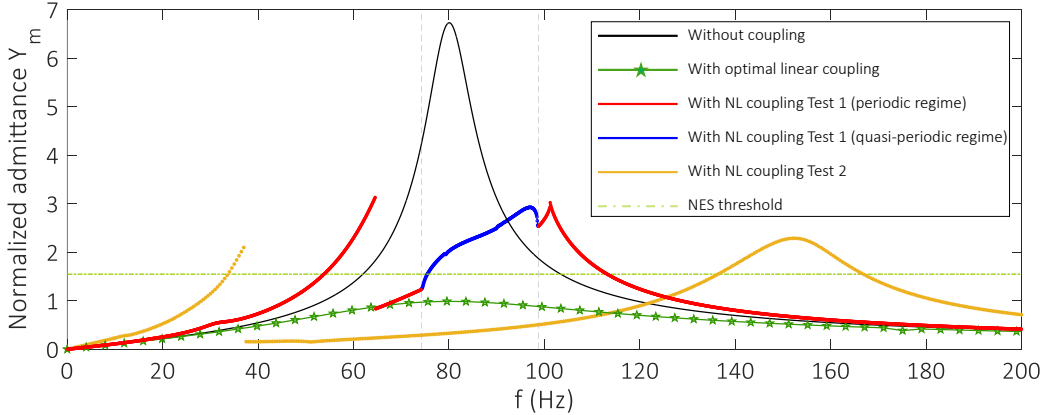


Figure 17: Comparison of the normalized admittance as function of frequency between the cases of open circuit, optimal linear resistor and the shunt nonlinear circuits. Test 1 for $L_p = 132$ dB and Test 2 for $L_p = 115$ dB both for $k = 3468 \text{ V}^{-2}$.

466 Figure 17 shows the normalized admittance Y_m according to frequency
 467 $f(\text{Hz})$. Black curve line represents the case when the electroacoustic trans-
 468 ducer is not connected to any electric load, where its corresponding absorp-
 469 tion coefficient present a maximum value α_{max} which is smaller than 1 at the
 470 resonance. Stars dashed curve illustrates the case when plugging a positive
 471 optimal resistor R_{opt} that can be obtained by the following formula [8]

$$R_{opt} = \frac{(Bl)^2}{Z_{mc} - R_{ms}} - R_e \text{ with } Z_{mc} = \rho c S \quad (36)$$

472 Remarkably, the shunt resistor permits a significant decrease in the nor-
 473 malized admittance with a perfect absorption at the resonance. However,
 474 this approach is limited to a narrow range of frequency with no possible
 475 broadening control of the bandwidth.

476 Regarding the behavior of the system when connecting a nonlinear elec-
 477 tric shunt circuit; the curve illustrated in crosses represents the \mathbf{L}_2 -norm of
 478 the normalized acoustic admittance when reaching a periodic regime. Quasi-
 479 periodic regime illustrating the maximum of peaks absolute values is repre-
 480 sented with dark circles. Remarkably, it exists in the vicinity of the resonance
 481 frequency ω_0 and can be identified by the vertical black dashed lines.

482 In the vicinity of 1:1 resonance, an optimal response frequency of the
 483 system can be identified through a selected threshold. It corresponds to the
 484 maximum of energy that the primary system can reach during an energy

485 exchange process with the NES. Thus, the optimal design defined in terms
 486 of normalized admittance is represented by the horizontal dash-dotted light
 487 line.

488 Remarkably, the added passive nonlinear shunt circuit allowed a signifi-
 489 cant decrease of the admittance, principally at the vicinity of the resonance
 490 frequency where the TET prevents the velocity to exceed a certain ampli-
 491 tude. Moreover, we can identify that the frequency bandwidth undergoes a
 492 45% of relative increase.

493 The sound absorption coefficient is usually used as a performance indi-
 494 cator for linear studies to optimize its bandwidth. However, underlining the
 495 fact that with the nonlinear coupling, this coefficient may not be necessar-
 496 ily appropriate since the interest of the nonlinear targeted energy transfer
 497 is mainly to highly-energetic non-stationary regimes. Moreover, it does not
 498 reflect the different responses of such systems (strong modulated responses,
 499 modal exchanges. . .). Then, we choose to apply the following expression of
 500 the sound absorption coefficient α , defined for periodic regimes only as

$$\alpha(\omega) = 1 - |r(\omega)|^2 \quad (37)$$

501 with $|r(\omega)|$ defining the magnitude of the following reflection coefficient

$$r(\omega) = \frac{1 - Y_m(\omega)}{1 + Y_m(\omega)}. \quad (38)$$

502 As done by some authors in the nonlinear field ([28, 29]) we choose to
 503 illustrate certain properties of the nonlinear shunt circuits compared to clas-
 504 sical linear ones, highlighting the performance of the sound absorption just
 505 for periodic regime (the sound absorption coefficient is not defined for quasi-
 506 periodic ones). Figure 18 shows a comparison of the sound absorption co-
 507 efficient between the different treated cases (without coupling, with linear
 508 optimal resistor and nonlinear shunt circuits). We should note that for the
 509 nonlinear shunt circuit using the physical parameters of Test 2, the sound
 510 absorption was not defined during quasi-periodic regimes and thus not illus-
 511 trated between the vertical two dashed lines. Figure 18 highlights the fact
 512 that we managed to increase the controlled absorption bandwidth and ob-
 513 tain better absorption for low frequencies without an optimization study for
 514 now, even if we are less efficient than an optimal linear resistor around the
 515 resonance frequency.

516 We should highlight the fact that the absorption bandwidth can be controlled by choosing suitable passive nonlinear control parameters R_c , L_c , C
 517 and k .
 518

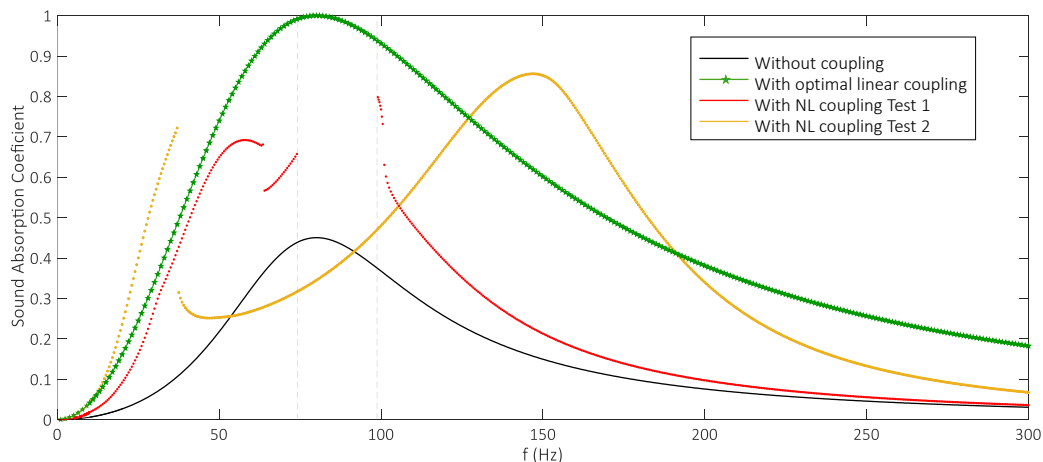


Figure 18: Comparison of the sound absorption coefficient as function of frequency between the cases of open circuit, optimal linear resistor, the shunt nonlinear circuits Test 1 for $L_p = 132$ dB and Test 2 for $L_p = 115$ dB both for $k = 3468 \text{ V}^{-2}$.

519 6.4.2. Remarks and interpretations

520 The present approach uses the complexification of Manevitch for the case
 521 of 1:1 resonance. Then, in the vicinity of ω_0 this approach presents a pre-
 522 dictive tool allowing an analytical identification of the desirable regime for a
 523 give sound pressure level and a selected frequency. An optimal NES design
 524 can be identified when the system response does not exceeded the chosen
 525 threshold. However, for the present physical parameters, Figure 17 displays
 526 a slight difference between the admittance maximum amplitude in the quasi-
 527 periodic regime and the horizontal threshold. This gap can be due to several
 528 factors, among which we can mention the choice of the physical parameters.
 529 In addition, we used the classical Manevitch variables which only considers
 530 the first harmonics. An extended version of the complex variables is under
 531 investigations, for a finer approximation of the result.

532 7. Conclusion

533 A passive nonlinear passive shunt was coupled to the loudspeaker's termi-
 534 nals, playing the role of an electroacoustic absorber. The resulting structure

535 was described as a two dofs system, which was analytically treated using an
536 invariant manifold approach for the 1:1 resonance. The equilibrium points
537 and fold singularities were detected, allowing a predictive tool to design the
538 nonlinear passive shunt during the energy exchange process. The preliminary
539 results show that this approach is able to vary the acoustic properties of the
540 loudspeaker, with a relative reduction of the normalized admittance and a
541 broadening of the absorption frequency range.

542 Further work is dedicated to the design and optimization process of the
543 passive nonlinear shunt, which allows larger frequency bandwidth and higher
544 acoustic absorption performances. Moreover, we aim to extend the present
545 analytical approach for a finer investigations with larger frequency range(1:2,
546 2:1, . . . resonances). In practice, we aim to implement an experimental setup
547 in order to validate our analytico-numerical results.

548 **Acknowledgment**

549 This work was performed within the framework of the LABEX CeLyA
550 (ANR-10-LABX-0060) of Université de Lyon, within the program " Investisse-
551 ments d'Avenir » (ANR-16IDEX-0005) operated by the French National
552 Research Agency (ANR).

553 **Appendix A.**

554 Explicit values of variables in System (29) can be written as follows

$$\left\{ \begin{array}{l}
 \mathbf{A} = -\frac{\gamma}{\eta} \\
 \mathbf{B} = \frac{1}{\eta}(1 - \xi G(N_2^2))N_2 \\
 \mathbf{C} = -\frac{1}{\eta}(1 - \xi G(N_2^2) - 2\xi N_2^2 G'(N_2^2)) \\
 \mathbf{D} = -\frac{\gamma}{\eta}N_2 \\
 \mathbf{E} = \frac{1}{\eta} \left[\frac{\lambda\gamma}{2} + \frac{\alpha\eta}{2} - \sigma(1 - \xi G(N_2^2)) \right] N_2 + \frac{1}{2}f \cos(\delta_2) \\
 \mathbf{F} = \frac{1}{\eta} \left[\gamma\sigma + \frac{\lambda}{2}(1 - \xi G(N_2^2)) \right] N_2 - \frac{1}{2}f \sin(\delta_2)
 \end{array} \right. \quad (\text{A.1})$$

555 **References**

- 556 [1] J. P. Arenas and M. J. Crocker. Recent trends in porous sound-absorbing
557 materials. *Sound & Vibration*, 44:12–17, 2010.
- 558 [2] H. von Helmholtz. *Die Lehre von den Tonempfindungen als physiologische
559 Grundlage für die Theorie der Musik*. F. Vieweg und sohn, 1863.
- 560 [3] H. Frahm. Device for damping vibrations of bodies, 1909. U.S. Patent
561 No. 989958.
- 562 [4] M. Zilletti, S. J. Elliott, and E. Rustighi. Optimisation of dynamic
563 vibration absorbers to minimise kinetic energy and maximise internal
564 power dissipation. *Journal of Sound and Vibration*, 331(18):4093 – 4100,
565 2012.
- 566 [5] H. F. Olson and E. G. May. Electronic sound absorber. *The Journal of
567 the Acoustical Society of America*, 25(6):1130–1136, 1953.
- 568 [6] A. J. Fleming, D. Niederberger, S. O. R. Moheimani, and M. Morari.
569 Control of resonant acoustic sound fields by electrical shunting of a loud-
570 speaker. *IEEE Transactions on Control Systems Technology*, 15(4):689–
571 703, July 2007.
- 572 [7] F. Orduña Bustamante and P. A. Nelson. An adaptive controller for
573 the active absorption of sound. *The Journal of the Acoustical Society of
574 America*, 91(5):2740–2747, 1992.
- 575 [8] H. Lissek, R. Boulandet, and R. Fleury. Electroacoustic absorbers:
576 Bridging the gap between shunt loudspeakers and active sound absorp-
577 tion. *The Journal of the Acoustical Society of America*, 129(5):2968–
578 2978, 2011.
- 579 [9] Y. Zhang, Y.-J. Chan, and L. Huang. Thin broadband noise absorp-
580 tion through acoustic reactance control by electro-mechanical coupling
581 without sensor. *The Journal of the Acoustical Society of America*,
582 135(5):2738–2745, 2014.
- 583 [10] Jiancheng Tao, Ruixiang Jing, and Xiaojun Qiu. Sound absorption of
584 a finite micro-perforated panel backed by a shunted loudspeaker. *The
585 Journal of the Acoustical Society of America*, 135(1):231–238, 2014.

- 586 [11] Y. Zhang and L. Huang. Electroacoustic control of rijke tube instability.
587 *Journal of Sound and Vibration*, 409:131 – 144, 2017.
- 588 [12] Y. Lee, A. Vakakis, L. Bergman, D. M. McFarland, and G. Kerschen.
589 Suppression aeroelastic instability using broadband passive targeted en-
590 ergy transfers, part 1: Theory. *AIAA Journal*, 45(3):693 – 711, 2007.
- 591 [13] O. V. Gendelman, T. Sapsis, A. F. Vakakis, and L. A. Bergman. En-
592 hanced passive targeted energy transfer in strongly nonlinear mechanical
593 oscillators. *Journal of Sound and Vibration*, 330(1):1 – 8, 2011.
- 594 [14] T. P. Sapsis, D. Dane Quinn, A. F. Vakakis, and L. A. Bergman. Effec-
595 tive stiffening and damping enhancement of structures with strongly
596 nonlinear local attachments. *Journal of Vibration and Acoustics*,
597 134(1):011016–011016–12, 2012.
- 598 [15] N. Benarous and O. V. Gendelman. Nonlinear energy sink with com-
599 bined nonlinearities: Enhanced mitigation of vibrations and amplitude
600 locking phenomenon. *Proceedings of the Institution of Mechanical Engi-
601 neers, Part C: Journal of Mechanical Engineering Science*, 230(1):21–33,
602 2016.
- 603 [16] E. Gourdon, C. H. Lamarque, and S. Pernot. Contribution to efficiency
604 of irreversible passive energy pumping with a strong nonlinear attach-
605 ment. *Nonlinear Dynamics*, 50(4):793–808, Dec 2007.
- 606 [17] A. F. Vakakis, O. V. Gendelman, L. A. Bergman, D. M. McFarland,
607 G. Kerschen, and Y. S. Lee. *Nonlinear Targeted Energy Transfer in Me-
608 chanical and Structural Systems*. Solid Mechanics and Its Applications.
609 Springer Netherlands, 2008.
- 610 [18] E. Gourdon, N. A. Alexander, C. A. Taylor, C. H. Lamarque, and S. Per-
611 not. Nonlinear energy pumping under transient forcing with strongly
612 nonlinear coupling: Theoretical and experimental results. *Journal of
613 Sound and Vibration*, 300(3):522 – 551, 2007.
- 614 [19] R. Bellet, B. Cochelin, P. Herzog, and P.-O. Mattei. Experimental study
615 of targeted energy transfer from an acoustic system to a nonlinear mem-
616 brane absorber. *Journal of Sound and Vibration*, 329(14):2768 – 2791,
617 2010.

- 618 [20] E. Rivet, S. Karkar, and H. Lissek. Multi-degree-of-freedom low-
619 frequency electroacoustic absorbers through coupled resonators. *Applied*
620 *Acoustics*, 132:109 – 117, 2018.
- 621 [21] O. V. Gendelman. Targeted energy transfer in systems with external and
622 self-excitation. *Proceedings of the Institution of Mechanical Engineers,*
623 *Part C: Journal of Mechanical Engineering Science*, 225(9):2007–2043,
624 2011.
- 625 [22] H. Lissek, R. Boulandet, and E. Rivet. Optimization of electric shunt
626 resonant circuits for electroacoustic absorbers. In Société Française
627 d’Acoustique, editor, *Acoustics 2012*, Nantes, France, April 2012.
- 628 [23] O. V. Gendelman, E. Gourdon, and C.-H. Lamarque. Quasiperiodic
629 energy pumping in coupled oscillators under periodic forcing. *Journal*
630 *of Sound and Vibration*, 294(4-5):651–662, July 2006.
- 631 [24] L. I. Manevitch. The description of localized normal modes in a chain
632 of nonlinear coupled oscillators using complex variables. *Nonlinear Dy-*
633 *namics*, 25(1):95–109, Jul 2001.
- 634 [25] A. Ture Savadkoohi, C.-H. Lamarque, and Z. Dimitrijevic. Vibratory en-
635 ergy exchange between a linear and a nonsmooth system in the presence
636 of the gravity. *Nonlinear Dynamics*, 70(2):1473–1483, Oct 2012.
- 637 [26] M. Weiss, A. Ture Savadkoohi, O. V. Gendelman, and C.-H. Lamar-
638 que. Dynamical behavior of a mechanical system including saint-venant
639 component coupled to a non-linear energy sink. *International Journal*
640 *of Non-Linear Mechanics*, 63:10–18, 2014.
- 641 [27] T. A. Nguyen and S. Pernot. Design criteria for optimally tuned non-
642 linear energy sinks—part 1: transient regime. *Nonlinear Dynamics*,
643 69(1):1–19, Jul 2012.
- 644 [28] Y. Y. Lee. Analytic formulation for the sound absorption of a panel
645 absorber under the effects of microperforation, air pumping, linear
646 vibration and nonlinear vibration. *Abstract and Applied Analysis*,
647 2014(906506):–, 2014.
- 648 [29] Y. Y. Lee, Q. S. Li, A. Y. T. Leung, and R. K. L. Su. The jump
649 phenomenon effect on the sound absorption of a nonlinear panel absorber

650 and sound transmission loss of a nonlinear panel backed by a cavity.
651 *Nonlinear Dynamics*, 69(1):99–116, Jul 2012.